Chapter 2

NANOMEMS PHYSICS: QUANTUM WAVE-PARTICLE PHENOMENA

2.1 Introduction

As discussed in Chapter 1, NanoMEMS aims at exploiting the convergence between nanotechnology and microelectromechanical systems (MEMS) brought about by advances in the ability to fabricate nanometer-scale electronic and mechanical device structures. This novel paradigm, in turn, poses an interesting challenge from the device physics point of view. In particular, the invention and/or discovery of a plethora of new materials, concepts and techniques such as carbon nanotubes (CNTs) [17], photonic band-gap crystals (PBCs) [51], and MEMS [52-55], respectively, has opened up new possibilities to implement novel devices upon which a new "electronics" technology, with attributes that are far superior to everything known to date, may be predicated. With the simultaneous convergence and exploitability, at such small length scales (e.g., down to a few nanometers), of various types of physical properties and effects, for instance, electronic, mechanical, optical, and magnetic and quantum effects, the nature of the concomitant new universe of devices and circuits that will fuel this new electronics will clearly be vast, yet, it is at present mostly unknown. In this context, many domains of physics, not usually invoked in describing the behavior of prior-art devices, become simultaneously pertinent. Such elements include [56], the manifestation of charge discreteness, the quantum electrodynamical (QED) *Casimir effect,* quantized heat flow, manifestation of the wave nature of electrons, quantum information theory, computing and communications, wave behavior in periodic and non-periodic media, and quantum squeezing. In this chapter, and the following, we expose fundamental knowledge required to analyze devices exploiting these phenomena.

2.2 Manifestation of Charge Discreteness

2.2.1 Effects of Charge Discreteness in Transmission Lines

The most fundamental element in circuits and systems is the interconnect or transmission line (TL). TLs play an essential role in configuring circuits and systems at all length scales [56]. Ideally, TLs are the medium through which signals propagate, from one point to another, with no effect on the signals, except a frequency-independent delay. Figure 2-1 shows a sketch of a microstrip TL, a commonly used TL in integrated circuits. It consists of a metallic stripe of width w and thickness t_s, patterned on a dielectric substrate of thickness h and dielectric constant ε_r, with the substrate resting on a metallic ground plane.

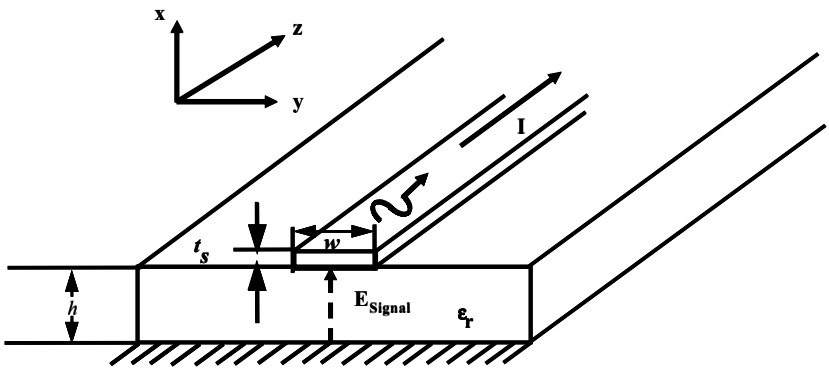

Figure 2-1 Sketch of microstrip transmission line.

From an electromagnetics perspective, the TL's qualitative operation is simple [57]. The signal of interest is impressed at its input, by way of its equivalent electric field E_{Signal} between the metallic stripe and the ground plane, and it elicits a propagating quasi-TEM electromagnetic wave which is guided in the dielectric substrate region between the stripe and the ground plane. A current I, flowing in one direction in the stripe, and in the opposite direction in the ground plane, embodies the boundary conditions necessary to sustain the propagating wave in the substrate, as per Maxwell's equations [57], and the magnitudes of the magnetic and electric fields stored along the line give rise to an inductance per unit length, L, and a capacitance per unit length, C, whose ratio is captured in the so-called characteristic impedance of the line, given by $Z_0 = \sqrt{L/C}$. TLs are usually designed to have $Z_0 = 50\Omega$, which results if, for example, $h = 635\mu m$, $w = 635\mu m$,

$t_s = 2\mu m$, and $\varepsilon_r = 9.8$. Under these conditions of a metal stripe of relatively large dimensions with respect to a Bohr radius, a_0=0.592Å=0.0592nm, the current *I* may be construed as consisting of an ensemble of freely-propagating electrons, each characterized by a plane wave-*like* wave function $\psi \sim e^{ikz}$, with *continuous* energy $E = \hbar^2 k^2 / 2m^*$, where $\hbar$ is Planck's constant, $k = 2\pi/\lambda$ is the wave vector, λ the electron wavelength, and *m** the effective mass [58].

Assuming a lossless TL, its circuit behavior may be represented as a tandem connection of a number of finite-length cells, each cell consisting of a length Δz of its inductance, L, and capacitance, C, per unit length, see Figure 2-2(a) [56].

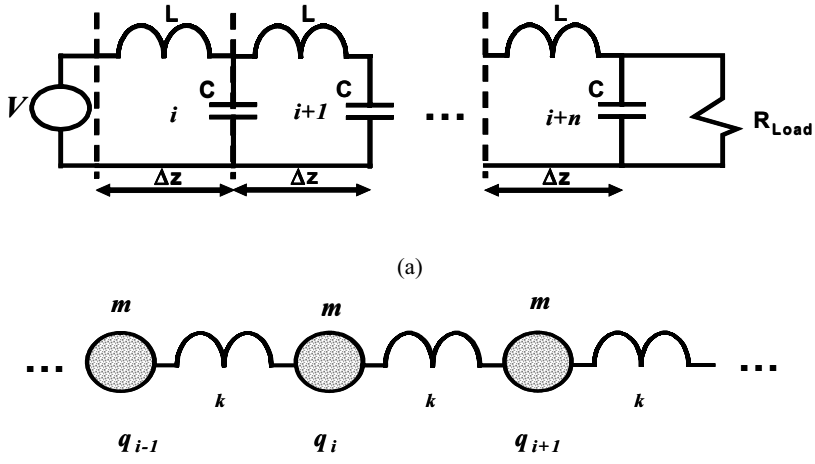

Figure 2-2. (a) Model of ideal transmission line. (b) Model of monatomic linear chain.

Thus, the propagation of a signal from a source towards a load, down a TL, can be visualized as an advancing tide of *charge fluid* charging the successive cells until the load is reached.

Enter nanotechnology. In concert with exploiting the ability to pattern nanoscale circuits, it is expected that TLs with stripes of nanoscale and sub-nanoscale widths and thicknesses will be prominent. In this context, electron currents will be transported down very narrow and thin metallic wires, so narrow and thin, in fact, that their dimensions may stop at only tens of Bohr radii. This means that the electrons involved will not only experience quantum mechanical confinement, i.e., that their energy will become quantized and given by [58], [59]:

$$E \sim \frac{\hbar^2}{2m^*}\left[\left(\frac{\pi n_x}{t_s}\right)^2 + \left(\frac{\pi n_y}{w}\right)^2 + k_z^2\right] \tag{1}$$

but also, that their discrete nature will be manifest. This latter feature becomes operative when the system size along a transport dimension becomes of the order of the carrier inelastic coherence length, and it implies that, in addition to the quantum mechanical energy of confinement of Eq. (1), the Coulomb charging energy required for adding or removing an electron, $E_c = q^2/L_i$ where L_i is a characteristic length in direction *i*, must be taken into account [58-62]. One must then turn to quantum mechanics to properly describe the TL behavior.

The observation [61]-[63], that the charge q in successive cells, and the total energy, obey equations (2) and (3),

$$L\frac{d^2 q_i}{dt^2} = \frac{1}{C}\left(q_{i+1} + q_{i-1} - 2q_i\right) \tag{2}$$

$$H = \sum_i \left(\frac{1}{2L}\left(L\frac{dq_i}{dt}\right)^2 + \frac{1}{2C}\left(q_{i+1} - q_i\right)^2\right) \tag{3}$$

whose forms are *identical* to the equations describing the longitudinal vibration modes in a monatomic linear chain (MLC) [64] (see Appendix A), Figure 2(b), motivated the application of the quantum mechanical description of the latter to the TL. In particular, in (3), the first and second terms account for the magnetic and electric energies in the TL inductors and capacitors, respectively, and $p = L\frac{dq}{dt}$ and q play the roles of "momentum" and "coordinate," respectively. Notice, however, that since q is charge, p represents electric current.

The above TL quantization assumed the electric charge q to be a *continuous* variable. As has been observed [59], however, under appropriate circumstances, e.g., system size close to the inelastic coherence length, the particle (or *discrete*) nature of electrons becomes evident. Li [61] considered the consequences of this possibility and, accordingly, advanced a theory for TL quantization assuming q to be discrete.

The possibility of having the charge adopt exclusively discrete values, was introduced [61] by imposing the condition that the eigenvalues of the charge operator $\hat{q}$ be discrete, i.e.,

$$\hat{q}|q>=nq_e|q> \tag{4}$$

In other words, the result of measuring the charge in the TL must be *n* times the fundamental electron charge, q_e, where *n* is a positive *integer*. Since, from a comparison with the MLC description, charge adopts the role of a "coordinate" operator in the quantized Hamiltonian, the form of the corresponding "momentum" operator $\hat{p}$, and in particular,

$$\hat{p}^2=\left(\frac{\hbar}{i}\frac{\partial}{\partial q}\right)^2=-\hbar^2\frac{\partial^2}{\partial q^2} \tag{5}$$

must reflect this new situation. This is accomplished by replacing the partial derivative by its finite-difference approximation in charge coordinate space [65], i.e.,

$$\frac{\partial^2\psi}{\partial q^2}=\frac{\psi(n+1)-2\psi(n)+\psi(n-1)}{q_e^2} \tag{6}$$

where q_e is the fundamental unit discretizing the charge "axis" and ψ is the electron wavefunction in the charge representation. Assuming the line is driven by a voltage source *V*, Schrödinger's for the TL is given by Eq.(7) [61, 62]:

$$-\frac{\hbar^2}{2q_e^2L}\{\psi_{n+1}-2\psi_n+\psi_{n-1}\}+\left\{\frac{\hat{q}^2}{2C}+\hat{q}V\right\}\psi_n=\varepsilon\psi_n \tag{7}$$

or, using Eq. (4):

$$-\frac{\hbar^2}{2q_e^2L}\{\psi_{n+1}-2\psi_n+\psi_{n-1}\}+\left\{\frac{q_e^2n^2}{2C}+Vq_en\right\}\psi_n=\varepsilon\psi_n. \tag{8}$$

Imposing charge discreteness, thus, turns Schrödinger's equation for a TL into a discrete, instead of a partial, differential equation.

The implications of charge discreteness are gauged from the nature of the corresponding eigenvalues and eigenvectors for this equation. Obtaining these becomes more transparent upon developing the quantum theory of mesoscopic TLs [61, 62], which we outline below following Li [61].

With $\hat{q}$ as the charge operator, instead of the conventional spatial coordinate, the corresponding conjugate variable is taken as $\hat{p}$, which then represents the current operator, instead of the usual momentum operator. The quantum mechanics of the TL then evolves from (8) and the commutation relation:

$$[\hat{q}, \hat{p}] = i\hbar . \tag{9}$$

The fact that the eigenstates of $\hat{q}$ must be specified by an integer, *n*, allows two consecutive states to be related to one another by the application of a shift operator, in particular, $\widetilde{Q} \equiv e^{iq_e \hat{p}/\hbar}$. By expanding the exponential, and using (4) and (9), this shift operator may be shown to obey the commutation relations:

$$[\hat{q}, \widetilde{Q}] = -q_e \widetilde{Q} \tag{10}$$

$$[\hat{q}, \widetilde{Q}^+] = q_e \widetilde{Q}^+ \tag{11}$$

$$\widetilde{Q}^+ \widetilde{Q} = \widetilde{Q} \widetilde{Q}^+ = 1 . \tag{12}$$

The shift operator, when applied to the number eigenstates defined by, $\hat{q}|n> = nq_e|n>$, produces the following new states:

$$\widetilde{Q}^+ |n> = e^{i\alpha_{n+1}} |n+1> \tag{13}$$

$$\widetilde{Q} |n> = e^{i\alpha_n} |n-1> \tag{14}$$

where $\alpha_n s$ are undetermined phases. Therefore, (13) and (14) lead to the interpretation of the shifter operators $\widetilde{Q}^+$ and $\widetilde{Q}$ as ladder operators that increase and decrease the charge of the charge operator in its diagonal representation.

The quantization apparatus is completed when the completeness and orthogonality relations, and the inner product are stipulated, in this case as given by (15)-(17), respectively,

$$\sum_n |n><n| = 1 , \tag{15}$$

$$< n|m >= \delta_{nm}, \tag{16}$$

$$< \phi|\psi >= \sum_{n\in Z} < \phi|n >< n|\psi >= \sum_{n\in Z} \phi^*(n)\psi(n), \tag{17}$$

where *n* belongs to the set of non-negative integers Z.

These relationships permit obtaining the fundamental quantum mechanical properties of the TL, namely, the eigenfunctions of the "momentum" operator $\hat{p}$, i.e., the nature of the current, and the energy spectrum.

Assuming the usual relations [53], $\hat{p}|p >= p|p >$ and $f(\hat{p})|p >= f(p)|p >$, Li [62] expands the momentum states in terms of the number states, $|p >= \sum_{n\in Z} c_n(p)|n >$ together with the shifting operation $\widetilde{Q}|p >= e^{iq_e\hat{p}/\hbar}|p >$, to obtain the relationship $c_{n+1}/c_n = \exp(iq_e p/\hbar + i\alpha_{n+1})$. This, in turn, yields the momentum expansion in terms of the number states as,

$$|p >= \sum_{n\in Z} \kappa_n e^{inq_e p/\hbar}|n > \tag{18}$$

where $\kappa_n = e^{i\sum_{j=1}^{n}\alpha_j}$ and $\kappa_{-n} = e^{-i\sum_{j=1}^{n}\alpha_{-j}}$ for *n*>0. Making the substitution $p \to p + \hbar(2\pi/q_e)$ in the exponential of (18) yields the same state $|p >$, from where it is determined that the momentum operator $\hat{p}$ is periodic. Further progress towards obtaining the eigenstates and dispersion is attained by noticing that, if one defines new discrete derivative operators by:

$$\nabla_{q_e}\psi(n) = \frac{\psi(n+1) - \psi(n)}{q_e}, \tag{19}$$

$$\overline{\nabla}_{q_e}\psi(n) = \frac{\psi(n) - \psi(n-1)}{q_e}, \tag{20}$$

then Schrödinger's equation (8), may be expressed as:

$$-\frac{\hbar^2}{2q_e^2 L}\left\{\left\{\nabla_{q_e} - \overline{\nabla}_{q_e}\right\} + \left\{\frac{\hat{q}^2}{2C} + V\hat{q}\right\}\right\}\psi = \varepsilon\psi, \tag{21}$$

from where a momentum operator $\hat{P}$, given by:

$$\hat{P} = \frac{\hbar}{2i}\left(\nabla_{q_e} + \overline{\nabla}_{q_e}\right) = \frac{\hbar}{2iq_e}\left(\widetilde{Q} - \widetilde{Q}^{+}\right), \tag{22}$$

may be defined. This new momentum operator is related to $\hat{p}$ in that $\hat{p} = \lim_{q_e \to 0} \hat{P}$.

2.2.1.1 Inductive Transmission Line Behavior

Inductive behavior is displayed by the so-called pure L-design, in which the TL is considered to have very narrow width (high impedance). Its mathematical description is given by:

$$\hat{H}_0 = -\frac{\hbar^2}{2q_e^2 L}\left\{\nabla_{q_e} - \overline{\nabla}_{q_e}\right\}, \tag{23}$$

where the terms involving the line capacitance is neglected and the driving voltage is set to zero. With this definition, and taking into account the relationship $\widetilde{Q}|p> = e^{iq_e\hat{p}/\hbar}|p>$, the following relationships are obtained:

$$\hat{P}\left|p\right> = \frac{\hbar}{q_e}\sin\left(\frac{q_e p}{\hbar}\right)\left|p\right>, \tag{24}$$

and

$$\hat{H}_0\left|p\right> = \frac{\hbar^2}{q_e^2 L}\left(1 - \cos\left(\frac{q_e p}{\hbar}\right)\right)\left|p\right>, \tag{25}$$

These are the desired momentum eigenstates and the energy spectrum. What is clear from (24) is that the current in a mesoscopic inductive line, given by $I = \hat{P}/L$, is periodic, becomes zero whenever $p = 2\pi\hbar/q_e$; $q_e \neq 0$, and that it is bounded by $\left(-\hbar/q_e L, \hbar/q_e L\right)$. Similarly, from (25) it is determined that the lowest energy state is degenerate at $p = n\hbar/q_e$.

Another peculiarity of mesoscopic TLs is the nature of their energy spectrum when formed into a ring in the presence of a magnetic flux ϕ. In this case, Schrödinger's becomes,

$$-\frac{\hbar^2}{2q_e^2 L}\left\{D_{q_e}-\overline{D}_{q_e}\right\}\psi=\varepsilon\psi, \tag{26}$$

where D_{q_e} and $\overline{D}_{q_e}$ are discrete derivatives that remain covariant in the presence of the magnetic flux ϕ and are defined by Li [61] as,

$$D_{q_e}\equiv e^{-\frac{q_e}{\hbar}\phi}\frac{\widetilde{Q}-e^{\frac{iq_e}{\hbar}\phi}}{q_e}\;;\;\overline{D}_{q_e}\equiv e^{-\frac{q_e}{\hbar}\phi}\frac{e^{\frac{-iq_e}{\hbar}\phi}-\hat{Q}^{+}}{q_e}. \tag{27}$$

Applying the Hamiltonian in (26) to the eigenstate $|p>$, the energy eigenvalues are obtained as,

$$\varepsilon(p,\phi)=\frac{2\hbar}{q_e^2}\sin^2\left(\frac{q_e}{2\hbar}(p-\phi)\right), \tag{28}$$

where ϕ is the magnetic flux threading the TL. Thus, (28) implies that when the discrete nature of charge is at play, the TL energy becomes a periodic function of p or ϕ, with maximum amplitude $\frac{2\hbar}{q_e^2}$ and nulls occurring whenever $p=\phi+n\hbar/q_e$. Furthermore, it has also been shown that the TL current is given by,

$$I(\phi)=\frac{\hbar}{q_e L}\sin\left(\frac{q_e}{\hbar}\phi\right), \tag{29}$$

which implies that it becomes an oscillatory function of the magnetic flux. Since no applied forcing function was assumed, (29) leads to the important observation [62] that a TL in the discrete charge regime will, in the presence of a magnetic flux, exhibit *persistent currents* [59]. These are currents without dissipation, such as the atomic orbital currents that elicit orbital magnetism.

2.2.1.2 Capacitive Transmission Line Behavior

In this design the TL is capacitive (low-impedance) and the first bracketed term in (21) is neglected and the Schrödinger equation is given by,

$$-\frac{\hbar^2}{2q_e^2 L}\left\{\frac{\hat{q}^2}{2C}+V\hat{q}\right\}\psi=\varepsilon\psi\,, \tag{30}$$

In this case, the Hamiltonian operator commutes with the charge operator $\hat{q}$, and consequently [60], they have simultaneous eigenstates. In particular, the energy of the state $|n>$ is given by [67],

$$\varepsilon=\frac{1}{2C}\left(nq_e-CV\right)^2-\frac{C}{2}V^2\,, \tag{31}$$

where *n* is the number of elemental charges describing the TL state. Thus, (31) implies that when the discrete nature of charge is at play in a low-impedance line, the TL energy is a quadratic function of the state *n* of charges.

An interesting phenomena is predicted for the current flow. In particular, as the applied voltage increases, the TL charge can only increase in discrete steps which are a multiple of q_e. Since the voltage required to cause this charge to be injected into the TL is q_e/C, it can be said that the voltage axis is quantized in units of q_e/C. Thus, the total charge of a line in the ground state is given by [67],

$$q=\sum_{k=0}^{\infty}\left\{u\left[V-\left(k+\frac{1}{2}\right)\frac{q_e}{C}\right]-u\left[-V-\left(k+\frac{1}{2}\right)\frac{q_e}{C}\right]\right\}q_e\,, \tag{32}$$

where *u(z)* is the unit step function. Consequently, by taking the time derivative of (32), one obtains the corresponding current as,

$$I=\frac{dq}{dt}=\sum_{k=0}^{\infty}q_e\left\{\delta\left[V-\left(k+\frac{1}{2}\right)\frac{q_e}{C}\right]+\delta\left[V+\left(k+\frac{1}{2}\right)\frac{q_e}{C}\right]\right\}\frac{dV}{dt}\,. \tag{33}$$

Eqn. (33) indicates that the current exhibits a series of *delta-function* impulses with periodicity q_e/C, consistent with every time a single electron

charge is added, and amplitude proportional to the slope of the voltage source. This leads to the important observation [67] that a low-impedance ideal TL in the discrete charge regime will exhibit current flow dominated by *Coulomb blockade*.

Clearly, as limiting cases, typifying the behavior of ideal high- and low-impedance TLs in the discrete charge regime, the phenomena of persistent currents and Coulomb blockade-type current flow, respectively, raise serious questions in the context of achieving low-noise analog and reliable digital circuits and systems at nanometric-length scales. As a result, complete awareness of the possibility that these features might be inadvertently included in the design space must be incorporated in TL/interconnect models utilized in the design and analysis of future NanoMEMS.

2.2.2 Effects of Charge Discreteness in Electrostatic Actuation

One of the distinguishing features of NanoMEMS is the inclusion of functions based on mechanical structures that can be actuated. For a variety of reasons, in particular, its compatibility with IC processes, electrostatic actuation is the actuation mechanism of choice for these devices [48], and is the one on which we focus our attention next.

2.2.2.1 Fundamental Electrostatic Actuation

Perhaps the most fundamental electrostatically-actuated elements/building blocks are the singly-(cantilever) and doubly-anchored beams [52], Figure 3.

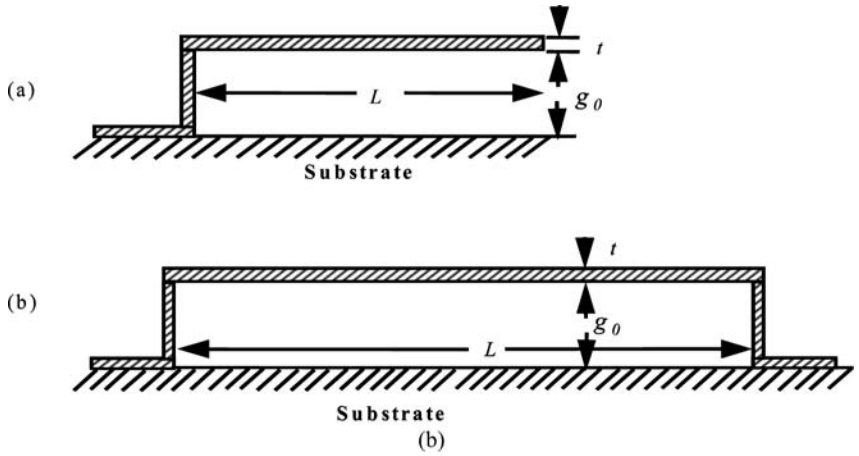

Figure 2-3. (a) Cantilever beam. (b) Doubly-anchored beam.

The devices are essentially parallel-plate capacitors, of nominal plate separation g_0, in which the top plate (beam) is free to move in response to an electrostatic force developed between it and the rigid bottom plate, as a result of a voltage applied between the two.

2.2.2.1.1 Large-signal Actuation—Switch

For typical dimensions employed in MEMS [48], e.g., beam gaps, lengths, widths, and thicknesses of about $2\mu m$, $100-250\mu m$, $10's\ of\ \mu m$, and $1-10\mu m$, respectively, the displacement behavior of the beams, which manifests itself as continuous gap reduction versus applied voltage, is dictated by the equilibrium $F_{Coulomb}+F_{Spring}=0$ established between the quadratic electrostatic force , $F_{Coulomb}=\frac{1}{2}\frac{\varepsilon_0 A V^2}{(g_0+z)^2}$, and the linear spring force, $F_{Spring}=-k_{Beam}z$, (Hooke's law) which attempts to bring the beam back to its undeflected position. This dynamic equilibrium, and its accompanying smooth displacement, is maintained up to about one-third of the beam-to-substrate distance, at which point it is lost and the beam collapses onto the bottom plate, abruptly reducing the gap to zero. The voltage demarcating these two regimes is called *pull-in* voltage and is given by [49],

$$V_{Pull-in}=\sqrt{\frac{8k_{Beam}g_0^{\ 3}}{27A\varepsilon_0}}, \tag{34}$$

where k_{Beam} is the spring constant of the beam, and A is the electrode area.

2.2.2.1.2 Small-signal Actuation—Resonator

For application as resonators [54], an AC voltage, together with a so-called DC polarization voltage, introduced to enhance the current elicited by the variable beam capacitance, are applied. Since the resonators are intended for application as stable frequency standards, with frequency given by [18],

$$f_{r,nom}=1.03\kappa\sqrt{\frac{E}{\rho}}\frac{h}{L_r^2}, \tag{35}$$

where κ is a scaling factor that models the effects of surface topography, including for instance, the anchor step-up and its corresponding finite elasticity, E is the Young's modulus of the beam material, ρ its density, h its thickness and L_r its length, the combined amplitude of AC and DC voltages is chosen to be lower than pull-in, thus keeping the beam from collapsing.

2.2.2.2 Coulomb Blockade

The phenomenon of Coulomb blockade [68, 69] refers to the fact that under certain conditions, namely, when junctions are defined whose capacitance is of the order of $C \sim 10^{-15} F$ or less, the energy required to increase the charge by one electron is not negligible with respect to temperature. For example [68], Figure 2.3 shows that, while a neutral metallic island, such as the plates of a capacitor, emits no electric field and, thus, allows the unimpeded approach of an electron, once this electron becomes part of the island it emits an electric field that may prevent the addition of more electrons.

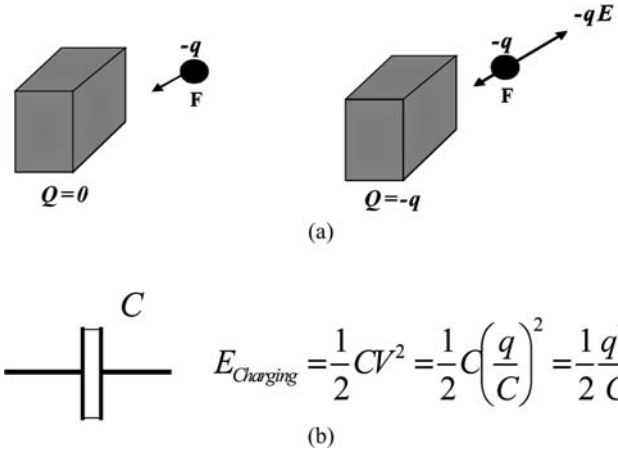

Figure 2-4. (a) Charging Coulomb island. (a) Charging energy of small capacitor.

At this point, the island *blocks* such an addition of extra charge. For a junction capacitance of $C \sim 10^{-15} F$, the minimum voltage required to add a charge q is q/C, thus the charging energy is $E_C = q^2/2C = 1.283 \times 10^{-23} J$, which is close to the thermal energy at 1K. If the capacitance were smaller, e.g., $C \sim 6.2 \times 10^{-18} F$, such as might be

typical for nanoparticles, then the charging energy would be close to the thermal energy at 300K. The implication of this is that it may be impossible to continuously inject charges into the capacitor when the charging energy exceeds the ambient temperature. Rather, for an increasing applied voltage, a charging event only occurs every time its magnitude exceeds the charging energy of an electron; one enters the Coulomb blockade regime and the current into the capacitor becomes pulse-like. The situation is illustrated in Figure 2-4 with respect to the so-called single-electron box [69].

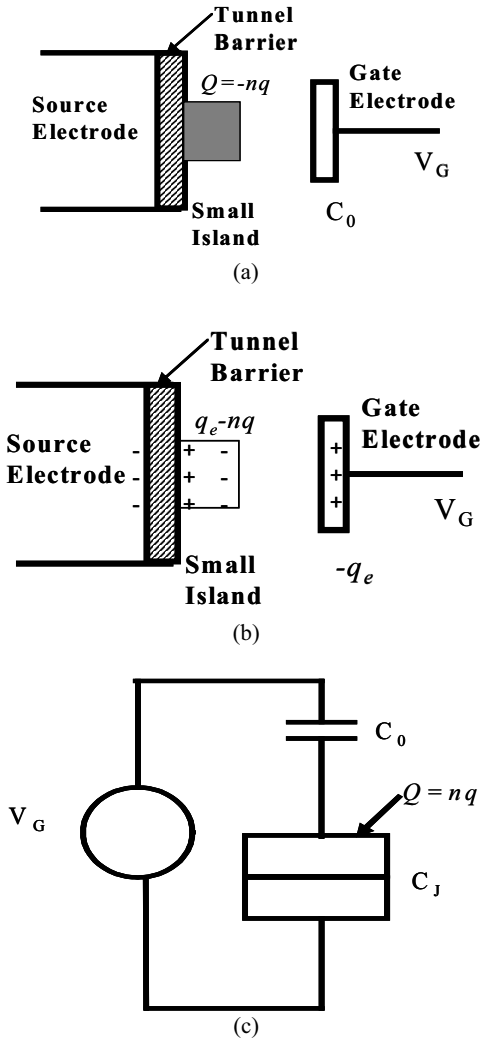

Figure 2-5. Voltage-controlled electron injection into metallic island. (a) V_G=0. (b) V_G>V_C. (c) Circuit model (*After* [68], [69].)

A voltage source V_G is connected through a small capacitor C_0, to a small metallic island that rests over a tunnel barrier which, in turn, is in contact with an electron reservoir. The capacitance of the tunnel barrier is denoted C_J, and the distance between the gate electrode and the small island, defining C_0, is such that tunneling is suppressed [69]. With V_G=0, the system is neutral; the small island containing *n* positive charges *q*, which are neutralized by an equal amount of negative charges -*nq*, Figure 2-24(a). When the gate voltage increases, the number of electrons in the small island may change by amounts $q_e = C_0 V_G$, Figure 2-4(b). In particular, the field induced by the gate causes an uncompensated charge *nq* to appear on the island. The capacitance "seen" by the island is C_0+C_J. Therefore, the charging energy accompanying the injection of a charge $q_e = C_0 V_G$ is,

$$E_C = \frac{(nq - q_e)^2}{2(C_0 + C_J)}, \tag{36}$$

It is noticed that, while the external charge q_e is continuous, the island charge may only increase in discrete steps of value *q*. Therefore, the island charge is a step-like function of the gate voltage. As a function of temperature, the average number of electrons in the island is given by [68] (37), Figure 2-5.

$$\langle n \rangle = \frac{\sum_{-\infty}^{\infty} n e^{-E_C/k_B T}}{\sum_{-\infty}^{\infty} e^{-E_C/k_B T}} \tag{37}$$

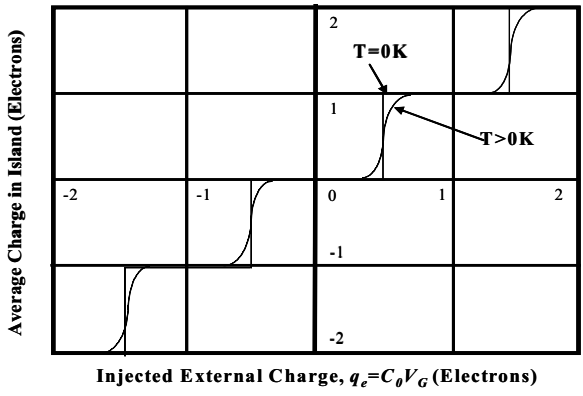

Figure 2-6. Average island charge versus injected charge. (*After* [69].)

2.2.3 Single-Electron Tunneling

Upon the island being populated by the injected charge, the charge tunnels through C_J and diffuses to the leads in a characteristic time τ given by the uncertainty principle (38) [69].

$$E_C \geq \frac{\hbar}{\tau}, \tag{38}$$

If the bias V_G causes the injection of a charge q every τ seconds, then a current of magnitude $I = q/\tau$ is set up, Figure 2-7.

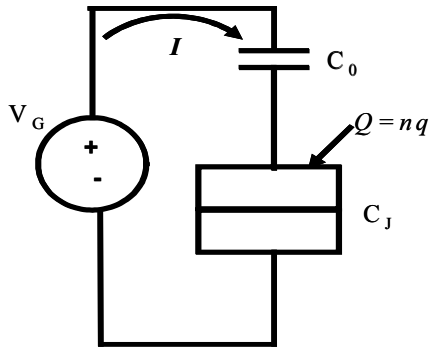

Figure 2-7. Single-electron tunneling schematic.

However, if this time is too short, then the current would appear to be continuous, as opposed to pulse-like. In this case, no discrete, single-electron tunneling event is observed. To observe single-electron tunneling, the characteristic time must exceed the product of the capacitance times the lead resistance, $\tau > RC$, a condition which leads to a minimum value for lead resistance, Eq. (38).

$$R > \frac{2\hbar}{q^2} \tag{38}$$

Notice that transport is occurring through a tunneling junction.

2.2.3.1 Quantum Dots

Quantum Dots (QDs) are structures in which electrons are confined in all three dimensions [59]. These structures include both gated layered structures

grown by MBE, and metal and semiconductor nanoparticles up to several nanometers, e.g., ~1-6 nm, in size. Because of their small size, which is comparable to that of the Bohr exciton, $a_{ex} = \varepsilon \cdot \hbar^2 / m_{ex} e^2$, electron energy levels in QDs are quantized. Electron transport through a QD is mediated by tunnel barriers, see Fig. 2-8, and is effected via a series of individual tunneling events across the barriers.

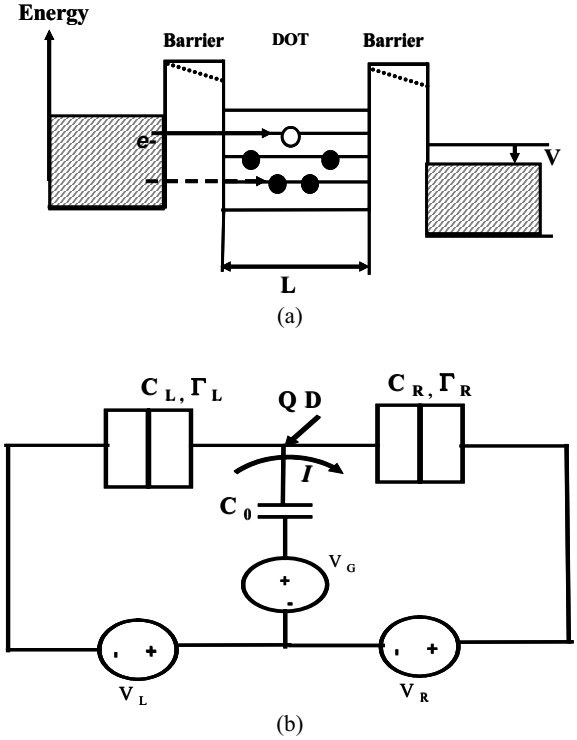

Figure 2-8. (a) Sketch of quantum dot energy level diagram. The continuous line denotes equilibrium, while the dashed line denotes reflects an applied voltage, V. The dashed arrow denotes suppressed current due to Coulomb blockade by QD electrons. (b) Equivalent circuit of QD.

The tunneling rate across the barriers is characterized by the change in free energy, Δ, resulting from the tunneling event, and the tunnel resistance, R_t ($R_t >> h/e^2$), and is given by [70], [71] Eq. (39).

$$\Gamma = \frac{\Delta}{e^2 R_t \left(1 - \exp\left(\frac{-\Delta}{k_B T}\right)\right)}. \tag{39}$$

In general, the tunneling rate will depend on the number of available (empty) states within the QD. If Γ_f is the tunneling rate into level *f* in the QD, g_f is the degeneracy factor, m_f is the number of electrons already occupying the level, and $F(\varepsilon) = 1/(1 + \exp(\varepsilon/k_B T))$ is the Fermi function, then the total tunneling rate is given by,

$$\Gamma_{QD}^{FS} = \sum_f \Gamma_f \cdot (g_f - m_f) F(\varepsilon_f^{QD} - \Delta), \tag{40}$$

where the initial and final electron energies are related by, $\varepsilon_i^{FS} = \varepsilon_f^{QD} - \Delta$, ε_i^{FS} being the initial electron energy [232], [233]. Notice that, at small bias voltages, the occupancy of QD states precludes tunneling due to Coulomb blockade.

2.2.4 Quantized Electrostatic Actuation

In contrast to conventional electrostatically-actuated MEM devices, which exhibit continuous displacement versus bias behavior prior to pull-in, the advent of precision nanoelectromechanical fabrication technology [72] and carbon nanotube synthesis [17] has enabled access to beams with dimensional features (gaps, lengths, widths, and thicknesses) of the order of several hundred nanometers in which conditions for the manifestation of charge discreteness become also evident. In fact, recent [73] theoretical studies of suspended (doubly anchored/clamped) carbon nanotubes (CNTs) in which Coulomb blockade dominates current transport have predicted that charge quantization in the CNTs will result in quantization of their displacement.

Specifically, Sapmaz, *et al*. [73] considered a single-wall nanotube (SWNT) modeled as a rod of radius *r*, and length *L*, separated by a gap g_0 over a bottom electrode, Fig. 2-9.

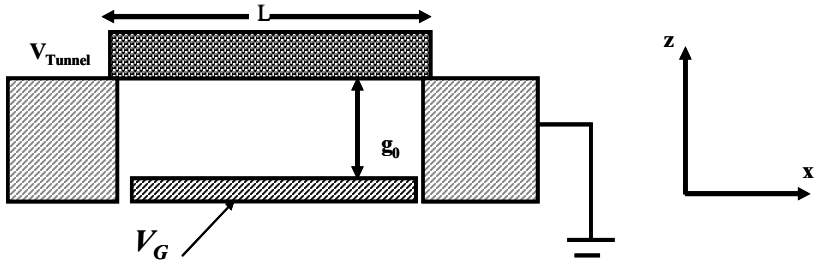

Figure 2-9. Schematic of suspended CNT as doubly anchored beam.

They described its behavior as follows. As the actuation voltage, V_G, applied between the CNT and the bottom electrode increases, the beam bends downwards causing the applied electrostatic energy to be converted into elastic deformation energy, given by,

$$U_{Elastic}[z(x)] = \int_0^L dx \left\{ \frac{EI}{2} z''^2 + \frac{\hat{T}}{2} z'^2 \right\}, \tag{41}$$

where E and $I = \pi r^4/4$ are the CNT Young's modulus and moment of inertia, respectively, and $\hat{T} = T_0 + T$ is total stress, comprised of the residual stress, T_0, and the stress induced by V_G, which is given by,

$$T = \frac{ES}{2L} \int_0^L z'^2 dx, \quad S = \pi r^2. \tag{42}$$

Since, ignoring residual stress, the beam elastic energy must correspond to the electrostatic energy that induced it, the total energy the state of deformed the beam arrives at is that at which the sum of elastic and electrostatic energies is a minimum. In the Coulomb blockade regime, however, as the bias voltage V is raised, a discrete number of charges, nq, populates the suspended CNT. Thus, the electrostatic energy must include this contribution, in addition to the actuation voltage (V_G)-induced deformation. Taking both electrostatic energy sources, into account, Sapmaz, *et al*. [73] approximated the total electrostatic energy by,

$$U_{Electrostatic}(z(x)) = \frac{(nq)^2}{2C_G(z)} - nqV_G \approx \frac{(nq)^2 \ln\frac{2R}{L}}{L} - \frac{(nq)^2}{L^2 R} \int_0^L z(x) dx \tag{43}$$

then, minimizing the total energy with respect to z, the following equation for the CNT bending was obtained,

$$IEz''' - Tz'' = F_0 = \frac{(nq)^2}{L^2 R}. \tag{44}$$

where F_0 is the electrostatic for per unit length. The bending of the doubly-anchored CNT, with the boundary conditions $z(0) = z(L) = z'(0) = z'(L) = 0$ was given as,

$$z(x)=\frac{F_0 L}{2T\xi}\left[\begin{array}{l}\dfrac{\sinh \xi L}{\cosh \xi L-1}(\cosh \xi L-1)- \\ \\ \sinh \xi x+\xi x-\xi \dfrac{x^2}{L}\end{array}\right], \quad \xi=\sqrt{\frac{T}{EI}}\,. \tag{45}$$

Finally, the effects of charge discreteness are manifest upon examining the maximum displacement as a function of actuation voltage, and given by (45) and (46).

$$z_{\max}=0.013\,\frac{(nq)^2 L^2}{Er^4 g_0}, \quad T<<\frac{EI}{L^2} \quad \left(n<<\frac{Er^5 g_0}{q^2 L^2}\right); \tag{46a}$$

$$z_{\max}=0.24\,\frac{(nq)^{2/3} L^{2/3}}{E^{1/3} r^2 g_0^{\,1/3}}, \quad T>>\frac{EI}{L^2} \quad \left(n>>\frac{Er^5 g_0}{q^2 L^2}\right) \tag{46b}$$

$$n=Int\left(\frac{V_G L}{2r\ln(2g_0/r)}+\frac{1}{2}+\delta n\right). \tag{47}$$

For a given applied voltage, (47) gives the value of n that minimizes the total energy, where δn is a small correction. Clearly, (45)-(47) reveal that the beam displacement is quantized, i.e., its position changes in discrete steps every time an electron tunnels into it.

2.3 Manifestation of Quantum Electrodynamical Forces

When the proximity between material objects becomes of the order of several nanometers, a regime is entered in which forces that are *quantum mechanical* in nature [74-76], namely, *van der Waals* and *Casimir forces*, become operative. These forces supplement, for instance, the electrostatic force in countering Hooke's law to determine the beam actuation behavior. They also may be responsible for stiction [77], i.e., causing close by elements to adhere together and, thus, may profoundly change actuation dynamics.

2.3.1 van der Waals Force

van der Waals forces, of electromagnetic and quantum mechanical origin, are responsible for intermolecular attraction and repulsion. When adjacent

materials [78] are separated by distances $R>>r$, where r is the atomic radius, the wave functions decay exponentially and no bonding forces are operative. At these distances, each molecule (atom) may be characterized as a dipole antenna emitting a fluctuating field with a frequency distribution characterized by an average frequency ϖ. For distances, R, smaller than the average emitted wavelength, i.e., $R < \bar{\lambda}$ or $\frac{R\varpi}{c} << 1$, the emitted fields are reactive in nature, i.e., they vary with distance as $\vec{E} \propto 1/R^3$. Therefore, with reference to two emitting molecules (atoms), separated a distance R and endowed with dipole operators $< \hat{d}_\omega >= \alpha E_\omega$, the van der Waals interaction energy between them derives from the self-consistent field induction at each others' site. In particular, atom 1 induces a field at the site of atom 2 given by, $\hat{E}_1^{ind}(2) \approx \hat{d}_1 / R^3$, which, in turn, induces a dipole at the site of atom 2 given by, $\hat{d}_2^{ind} = \alpha_2(\omega) \cdot \hat{d}_1 / R^3$, where $\alpha_2(\omega)$ is the polarizability at the site of atom 2. Similarly, the induced dipole at atom 2 induces a field at the site of atom 1 given by, $\hat{E}_2^{ind}(1) \approx \frac{\hat{d}_2}{R^3} \approx \alpha_2(\omega) \cdot \frac{\hat{d}_1}{R^6}$. Thus, the average ground state dipole energy of atom 1 is given by [78], $U_\omega(R) = < \hat{d}_1^* \cdot \hat{E}_1^{ind} >= \frac{\alpha_2}{R^6} < \hat{d}_1 \cdot \hat{d}_1^* >$ and is a function of its average dipole fluctuation. The signature of van der Waals forces is the $F_{vdW} = dU_{vdW} / dR \propto 1/R^7$ distance dependence.

For calculations, Desquesnes, Rotkin, and Aluru [79] have modeled the van der Waals energy by the expression,

$$U_{vdW}(R) = \int_{V_1} \int_{V_2} \frac{n_1 n_2 C_6}{R^6(V_1, V_2)} dV_1 dV_2, \tag{48}$$

where V_1 and V_2 embody two domains of integration of the adjacent materials, n_1 and n_2 are the densities of atoms pertaining to the domains V_1 and V_2, $R(V_1, V_2)$ is the distance between any point in V_1 and V_2, and C_6, with units $[eV\text{Å}^6]$, is a constant characterizing the interaction between atoms in materials 1 and 2. While a good first step for modeling purposes, the exclusively *pair wise* nature of the contributions embodied by (46) may not be accurate enough for tube geometry since it is known [80] that, in exact calculations, one needs to consider three-particle, four-particle, etc interactions, or equivalently multi-pole interactions. These multiple

interactions must be included to improve modeling results. Nevertheless, applied to a SWNT beam of diameter r and suspended by a gap R, they obtained the van der Waals energy per unit length of the CNT as,

$$\frac{U_{vdW}}{L} = \frac{C_6 \sigma^2 \pi^2 r(r+R)\left(3r^2 + 2(R+r)^2\right)}{2\left((R+r)^2 - r^2\right)^{7/2}}, \tag{49}$$

where $\sigma \cong 38 nm^{-2}$ is the atomic surface density, L is the CNT length. The corresponding van der Waals force is given by,

$$\begin{aligned} F_{vdW} &= \frac{d\left(\frac{U_{vdW}}{L}\right)}{dR} \\ &= \frac{-\left(C_6 \sigma^2 \pi^2 r \sqrt{R(R+2r)}\right) \cdot \left(8R^4 + 32R^3 r + 72R^2 r^2 + 80Rr^3 + 35r^4\right)}{2R^5 (R+2r)^5} \end{aligned} . \tag{50}$$

As mentioned previously, the van der Waals force is one contributor to the phenomenon of stiction. Thus, its prominence must be accounted for in the design of advanced structures, e.g., nanoelectromechanical *frequency tuning* systems [54] based on *quantum gears* [81], as estimates of its magnitude are useful in designing against it [18, 82].

2.3.2 Casimir Force

The Casimir force arises from the polarization of adjacent material bodies, separated by distances of less than a few microns, as a result of *quantum-mechanical fluctuations* in the electromagnetic field permeating the free space between them [74-77]. It may also arise if vacuum fluctuations are a classical real electromagnetic field [83]. The force may be computed as retarded van der Waals forces or as due to changes in the boundary conditions of vacuum fluctuations; these are equivalent viewpoints as far as it is known [80].

When the material bodies are parallel conducting plates, separated by free space, the Casimir force is attractive [74], however, in general whether the force is attractive or repulsive [82], [84] depends on both the boundary conditions, including specific geometrical features, imposed on the field as well as the relationship among material properties of the plates and the intervening space. For example, repulsive forces are predicted by

Lifshitz formula [75] if the material between two plates has properties that are intermediate between those of the plates.

The startling aspect of the Casimir force is that it is a manifestation of the purely quantum-mechanical prediction of *zero-point vacuum fluctuations* [74-77] (see Appendix A), i.e., of the fact that, even in circumstances in which the average electromagnetic field is zero, its average energy shows fluctuations with *small* but non-zero value, i.e., *there is virtually infinite energy in vacuum.* Research efforts aimed at the practical exploitation of this extremely large energy source, residing in free space, are under way [85-87].

Calculating the Casimir force entails circumventing the fact that the zero-point vacuum energy, $E_{Field} = \frac{1}{2}\hbar\sum_n \omega_n$ diverges, and many techniques to accomplish this have been developed [74-77], [88], [89], but including these in our presentation is well beyond the scope of this article. The essence of many of these calculations, however, is to compute the physical energy as a difference in energy corresponding to two different geometries, e.g., the parallel plates at a distance "*a*" apart, and these at a distance "*b*," where the limit as *b* tends to infinity is taken. For flat surfaces, the infinite part of the energy cancels when the energy difference of the two configurations is taken. The calculated zero-temperature Casimir energy for the space between two uncharged perfectly conducting parallel plates, Figure 2-10,

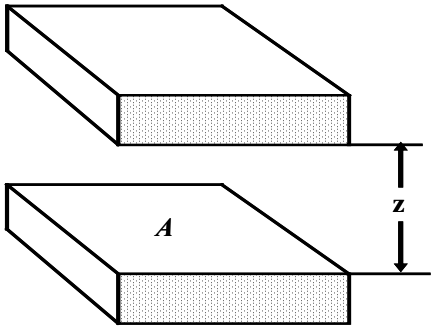

Figure 2-10. Casimir effect geometry.

is given by,

$$U_{Casimir}(z) = -\frac{\pi^2 \hbar c}{720}\frac{1}{z^3}, \tag{51}$$

and, the corresponding Casimir force per unit area is given by,

$$\frac{F_{Cas}^{0}}{A} = -\frac{\pi^2 \hbar c}{240}\frac{1}{z^4}. \tag{52}$$

For planar parallel metallic plates with an area $A = 1cm^2$ and separated a distance $z = 0.5\mu m$, the Casimir force is $2\times10^{-6}\,N$.

Many experiments measuring the Casimir force under various conditions, such as effecting normal displacement between a sphere and a smooth planar metal and between parallel metallic surfaces, as well as, effecting lateral displacement between a sphere and a sinusoidally corrugated surface, have been performed [89-95]. A good recent review of experiments and theory for Casimir forces has been published by Bordag, Mohideen, and Mostepanenko [89].

Since the Casimir energy/force is a sensitive function of the boundary conditions, corrections to the ideal expression (52) have been introduced to account for certain deviations. For example, for the sphere-plate geometry, the zero-temperature Casimir force is given by,

$$F^{0}_{Cas\_Sphere\text{-}Plate}(z) = -\frac{\pi^3}{360}R\frac{\hbar c}{z^3}, \tag{53}$$

where R is the radius of curvature of the spherical surface.

To include the finite conductivity of the metallic boundaries, two approaches have been advanced. In one, the force is modified as [96, 97],

$$F^{0,\sigma}_{Cas}(z) = F^{0}_{Cas\_Sphere-Plate}(z)\left[1 - 4\frac{c}{z\omega_p} + \frac{72}{5}\left(\frac{c}{z\omega_p}\right)^2\right], \tag{54}$$

where ω_p is the metal plasma frequency [64]. In the other, obtained by Lifshitz [98], the correction is ingrained in the derivation of the Casimir force, and is given by,

$$F^{0,\sigma}_{Cas}(z) = -\frac{R\hbar}{\pi c^3}\int_0^z dz'\int_0^\infty\int_1^\infty p^2\xi^3\,dp\,d\xi\times\left\{\left[\frac{(s+p)^2}{(s-p)^2}e^{\frac{2p\xi z}{c}}-1\right]^{-1}+\left[\frac{(s+p\varepsilon)^2}{(s-p\varepsilon)^2}e^{\frac{2p\xi z}{c}}-1\right]^{-1}\right\}, \tag{55}$$

where $s=\sqrt{\varepsilon-1+p^2}$, $\varepsilon(i\xi)=1+\frac{2}{\pi}\int_0^\infty \frac{\omega\varepsilon''(i\xi)}{\omega^2+\xi^2}d\omega$ is the dielectric constant of the metal, ε'' is the imaginary component of ε, and ξ is the imaginary frequency given by $\omega=i\xi$.

Corrections due to nonzero temperature yield [77],

$$F_{Cas}^{T}(z)=F_{Cas}^{0}(z)\left[1+\frac{720}{\pi^2}f(\zeta)\right], \tag{56}$$

where $\zeta=k_BTz/\hbar c$, k_B is Boltzmann constant, T is the absolute temperature, and

$$f(\zeta)\approx\begin{cases}(\zeta^3/2\pi)\vartheta(3)-(\zeta^4\pi^2/45), & for \quad \zeta\le 1/2\\ (\zeta/8\pi)\vartheta(3)-(\pi^2/720), & for \quad \zeta>1/2\end{cases}, \tag{57}$$

with $\vartheta(3)=1.202....$

Roy and Mohideen [90] included originally the effects of surface roughness, which changes the surface separation, by replacing the flat plate with a spatial sinusoidal modulation of period λ, and the energy averaged over the size of the plates, L, to obtain,

$$<U_{Casimir}\left(z+A\sin\frac{2\pi x}{\lambda}\right)>=-\frac{\pi^2\hbar c}{720}\frac{1}{z^3}\sum_m C_m\left(\frac{A}{z}\right)^m, \tag{58}$$

where A is the corrugation amplitude. The corresponding Casimir force is then given by the so-called, *Force Proximity Theorem* [99] relating the parallel plate geometry and the sphere-plate geometry, namely,

$$F_{Cas\_Roughness}=2\pi R<U_{Cas\_Rouchness}> \tag{59}$$

For $\lambda<<L$ and $z+z_0>A$, where z_0 is the average surface separation after contact due to stochastic roughness of the metal coating, they recommend the following coefficients in (58): $C_0=1$, $C_2=3$, $C_4=45/8$, $C_6=35/4$. A more accurate and general model for stochastic surface roughness, advanced by Harris, Chen, and Mohideen [88], includes the

effects of surface roughness, by replacing the flat plate with the mean stochastic roughness amplitude A, to obtain,

$$F_{Cas}^{r}(z) = F_{Cas}^{0}(z)\left[1+6\left(\frac{A}{z}\right)^{2}\right], \tag{60}$$

where A is derived from direct measurements via an Atomic Force Microscope (AFM).

2.4 Quantum Information Theory, Computing and Communications

The advent of nanoscale fabrication techniques has brought within our reach the possibility of producing systems whose predominant behavior is described by quantum mechanics (QM). While the engineering of systems based on exploting this new physics/technological paradigm is still in its infancy, this new paradigm is ultimately expected to manifest itself in the ushering of a 'new electronics' technology era. Obviously, this 'new electronics' is expected to change the way in which systems are implemented to effect the functions of information processing, computing and communications [100-111]. These functions, in turn, will exploit the properties of quantum mechanical wave functions. In this section we introduce key aspects of the fundamental physics on which these functions are predicated, in particular, we focus on the concepts underpinning quantum information processing, namely, quantum bits (*qubits*), quantum entanglement, the Einstein-Podolsky-Rosen (EPR) State, quantum gates, and quantum teleportation.

Quantum information is represented by quantum bits or *qubits* [103]. Qubits are fundamental physical entities, such as a two-level atom, which may adopt two possible quantum (stationary) states (see Appendix A), say the mutually orthogonal states $|0\rangle$ and $|1\rangle$. Due to its quantum nature, however, the most general state is expressed as,

$$|\psi\rangle = a|0\rangle + b|1\rangle, \tag{61}$$

i.e., as a superposition of both states. Thus, a measurement of the qubit will cause its wavefunction to *collapse* into the state $|0\rangle$ with probability $|a|^2$, or into the state $|1\rangle$ with probability $|b|^2$. This means that during its time evolution a qubit may be partly in both the $|0\rangle$ and $|1\rangle$ state at the same

time, i.e., to the degree that *a* and *b* may adopt an infinity of values, the qubit has the potential to be in *any* of these. A quantum system possessing *n* qubits is said to have 2^n accessible mutually orthogonal quantum states. For example, a system containing two noninteracting qubits will have the four states: $|00\rangle, |01\rangle, |10\rangle, |11\rangle$. States such as these, which represent the juxtaposition of independent or noninteracting systems (qubits), are called *tensor product* states.

2.4.1 Quantum Entanglement

In general, a tensor product provides the mathematical description of the state of a system that is constituted by bringing together noninteracting quantum systems, assuming that they remain without interacting [60]. Comprehending this concept is useful to get a clear understanding of the definition of an *entangled* state [107-111].

In particular, if associated with two quantum systems there are vector spaces V_1 of dimension N_1, in which resides a vector $|\phi\rangle$, and V_2 of dimension N_2, in which resides a vector $|\chi\rangle$, and where N_1 and N_2 may be finite or infinite, then the tensor product of V_1 and V_2 is denoted by the vector space V [60],

$$V = V_1 \otimes V_2, \tag{62}$$

of dimension $N_1 N_2$, where the vector,

$$|\phi\rangle \otimes |\chi\rangle = |\phi\rangle|\chi\rangle, \tag{63}$$

associated with the overall space V, is called the tensor product of $|\phi\rangle$ and $|\chi\rangle$.

If the vectors $|\phi\rangle$ and $|\chi\rangle$ can be expressed in terms of the respective bases $\{|u_i\rangle\}$ and $\{|v_i\rangle\}$, so that,

$$|\phi\rangle = \sum_i a_i |u_i\rangle, \tag{64}$$

and

$$|\chi\rangle = \sum_j b_j |v_j\rangle, \tag{65}$$

then, the tensor product may be written as,

$$|\phi\rangle \otimes |\chi\rangle = \sum_{i,j} a_i b_j |u_i\rangle \otimes |v_j\rangle, \tag{66}$$

from where it is seen that the components of a tensor product vector are the products of the components of the two vectors of the product. An example will help appreciate the meaning of a tensor product immediately. Let V_x and V_y be two vector spaces in which the bases $\{|x\rangle\}$ and $\{|y\rangle\}$, reside. Then the tensor product of the spaces is given by,

$$V_{xy} = V_x \otimes V_y, \tag{67}$$

and the tensor product of the bases is given by,

$$|xy\rangle = |x\rangle|y\rangle. \tag{68}$$

Consequently, if X and Y are operators in V_{xy}, then we have,

$$X|xy\rangle = X|x\rangle(|y\rangle) = x|x\rangle(|y\rangle) = x|x\rangle|y\rangle = x|xy\rangle, \tag{69}$$

$$Y|xy\rangle = (|x\rangle)Y|y\rangle = (|x\rangle)y|y\rangle = y|x\rangle|y\rangle = y|xy\rangle. \tag{70}$$

Essentially, then, the operators acting over a tensor product of spaces operate *only* on the vector space to which they belong.

Now, assume that the global state of the system is embodied by the wavefunction $|\psi\rangle \in V = V_1 \otimes V_2$. Then, according to the above, $|\psi\rangle = |\psi_1\rangle \otimes |\psi_2\rangle$, where $|\psi_1\rangle \in V_1$ and $|\psi_2\rangle \in V_2$. A quantum system is said to be *entangled* if it is impossible to express its global state as the tensor product, i.e., $|\psi\rangle \neq |\psi_1\rangle \otimes |\psi_2\rangle$. Thus, in an entangled system, it is not possible to act on one of its vector states independently without perturbing the others. It is said then, that the states in an entangled system are *correlated.*

2.4.1.1 Einstein-Podolsky-Rosen (EPR) State

In a system with two noninteracting qubits, the global state may be expressed as [108],

$$|\psi\rangle = c_1|00\rangle + c_2|01\rangle + c_3|10\rangle + c_4|11\rangle, \tag{71}$$

where $\sum_i |c_i|^2 = 1$ and each term is the tensor product of the components of the corresponding qubits. When $c_1 = c_4 = 0$, and $c_2 = c_3 = 1/\sqrt{2}$, the resulting state,

$$|\psi_{EPR}\rangle = \frac{(|01\rangle + |10\rangle)}{\sqrt{2}}, \tag{72}$$

is called an *EPR state* [108]. The EPR state is not a tensor product of the vector states, therefore, it represents an *entangled* state; it does not belong to any of the individual vector spaces, but is a combination of them. Associated with an EPR state is the so-called Bell-state basis [108], which embodies the possible states that can result upon measuring two-state quantum systems. In particular, if $|0\rangle_1$, $|1\rangle_1$ represent the two states of particle 1, and $|0\rangle_2$, $|1\rangle_2$ represent two states of particle 2, then the measurement of their EPR pair state may result in one of four state vectors, namely,

$$|\Psi^{\pm}\rangle = \frac{(|0\rangle_1|0\rangle_2 \pm |1\rangle_1|1\rangle_2)}{\sqrt{2}}, \tag{73}$$

and

$$|\Phi^{\pm}\rangle = \frac{(|0\rangle_1|1\rangle_2 \pm |1\rangle_1|0\rangle_2)}{\sqrt{2}}. \tag{74}$$

One of the most transparent demonstrations of entanglement and its implications was the experiment by Kwiat *et al*. [107], see Figure 2-11 below. This experiment exploited the principle of type-II parametric down conversion to produce directed beams of polarization entangled photons. In type-II parametric down conversion [107] an incident laser beam pump passes through a crystal, such as beta barium borate, and can spontaneously

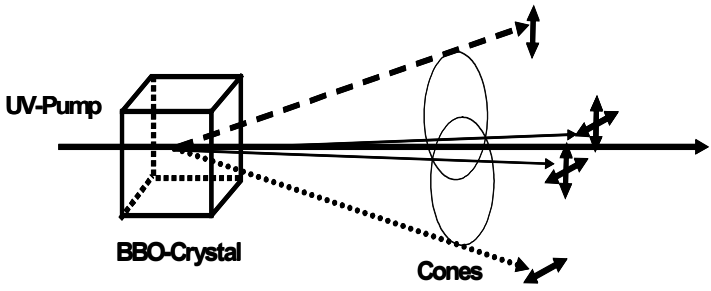

Figure 2-11. Entangled photons via type-II parametric down conversion. (*After* [107].)

decay into two photons of lower energy, one polarized vertically and one polarized horizontally, for instance. In particular, each photon can be emitted along a cone in such a way that two photons of a pair are found opposite to each other on the respective cones. If it occurs that the photons travel along the cone intersections, however, then neither photon is in a definite polarization state, but their relative polarizations are complementary, i.e., they are entangled. Taking the state of the photons along the intersecting cones as entangled, i.e.,

$$\left|\Phi^{-}\right\rangle = \frac{\left(\left|H\right\rangle_1\left|V\right\rangle_2 - \left|V\right\rangle_1\left|H\right\rangle_2\right)}{\sqrt{2}}, \tag{75}$$

we see that, because the polarization relationship of *complementarity* must be maintained, whenever photon 1 is measured and found to have vertical polarization, the polarization of photon 2 will be horizontal, and vice versa. This means that no matter the state in which photon 1 is found, the state of photon 2 can be predicted to be in the orthogonal state when measured. Entanglement, therefore, enables a strong correlation among the photons. This is a general property among entangled particles. By appropriately controlling the evolution of aggregates of particles, it is possible to induced them into entangled states. The agents that control the evolution of states are called *quantum gates*.

2.4.1.2 Quantum Gates

Given a qubit prepared in the initial state $\left|\psi(t_0)\right\rangle$, its state at a subsequent time t is given by $\left|\psi(t)\right\rangle = U(t,t_0)\left|\psi(t_0)\right\rangle$, where U is the qubit's *transition matrix*[60] Unitary *reversible* matrices U prescribing the evolution of qubits are called *quantum logic gates* [102], [111]. Thus, a

quantum gate transforming a qubit state such that $|0\rangle \rightarrow |0\rangle$ and $|1\rangle \rightarrow \exp(i\omega t)|1\rangle$, would have the form [102],

$$U(\theta) = \begin{bmatrix} 1 & 0 \\ 0 & e^{i\theta} \end{bmatrix}, \tag{76}$$

where $\theta = \omega t$. Since *U* is a unitary *reversible* transformation, the quantum gate must be reversible. This means that, given the output, one must be able to uniquely determine the value of the input. There are a number of important quantum gates of which *quantum information processing* systems are made of, namely, the identity gate [100-111],

$$|0\rangle \rightarrow |0\rangle, \tag{77}$$

$$|1\rangle \rightarrow |1\rangle, \tag{78}$$

the NOT gate,

$$|0\rangle \rightarrow |1\rangle, \tag{79}$$

$$|1\rangle \rightarrow |0\rangle, \tag{80}$$

the Z gate,

$$|0\rangle \rightarrow |0\rangle, \tag{81}$$

$$|1\rangle \rightarrow -|1\rangle, \tag{82}$$

and the Hadamard gate,

$$|0\rangle \rightarrow |0\rangle + |1\rangle, \tag{83}$$

$$|1\rangle \rightarrow |0\rangle - |1\rangle. \tag{84}$$

Quantum gates are represented graphically, as in Figure 2-12 [111]. In this figure the operation of the gate is read from left to right using the following convention. Each line represents the propagation or evolution of the input

state and could, accordingly, represent propagation via a wire, in time, in space, or in any other fashion evolution may be intended to take place. The gate has *control* qubits and *target* qubits. A control qubit, such as $|x\rangle$, has its line of propagation (wire) tapped at a dot. A target qubit, such as $|y\rangle$, has its line of propagation (wire) XOR'ed with a control bit. The gate's purpose is to effect a transformation on the target qubit based on the values of the control qubit, in particular, if the control qubit is set to one, then the target qubit is inverted. The realization of classical logic gates, which are inherently irreversible, by totally reversible quantum gates may be effected with the use of the Toffoli gate, see Figure 2-12(b). The Toffoli gate is an irreversible gate that takes three inputs, namely, two control qubits and one target qubit. By applying the Toffoli gate twice to its three input qubits, they are repoduced, thus the irreversible gate is made reversible [111].

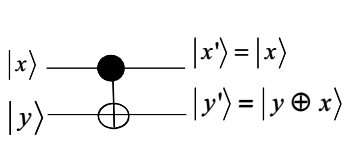

x	y	x'	y'
0	0	0	0
0	1	0	1
1	0	1	1
1	1	1	0

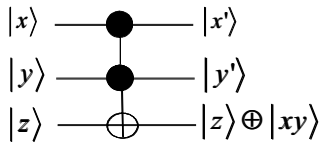

x	y	z	x'	y'	z'
0	0	0	0	0	0
0	0	1	0	0	1
0	1	0	0	1	0
0	1	1	0	1	1
1	0	0	1	0	0
1	0	1	1	0	1
1	1	0	1	1	0
1	1	1	1	1	1

(a) (b)

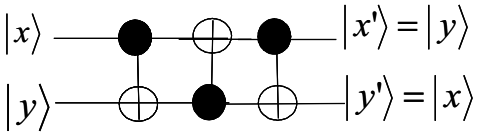

x	y	x'	y'
0	0	0	0
0	1	1	0
1	0	0	1
1	1	1	1

(c)

Figure 2-12. Truth tables and graphical representations of some quantum gates. (a) Control-NOT gate. (b) Control-control-NOT (Toffoli) gate. (c) Bit swapping.

The control-NOT (CNOT) gate, as can be seen from Figure 2-12(a), implements the exclusive-OR (XOR) operation. Thus, the gate inverts $|y\rangle$, if $|x\rangle = 1$, and leaves it as is if $|x\rangle = 0$. This operation is expressed as,

$$C_{12}|x\rangle|y\rangle = |x\rangle|(x+y)\bmod 2\rangle. \tag{85}$$

Applied to a pair of single product states of two qubits, the CNOT gate produces a set of entangled qubits, i.e.,

$$C_{12}(|0\rangle_1 + |1\rangle_1)|0\rangle_2 = (|0\rangle_1|0\rangle_2 + |1\rangle_1|1\rangle_2). \tag{86}$$

Similarly, since the CNOT gate is reversible, when applied to an entangled state, it produces a set of disentangled states, i.e.,

$$C_{12}(|0\rangle_1|0\rangle_2 \pm |1\rangle_1|1\rangle_2) = (|0\rangle_1 \pm |1\rangle_1)|0\rangle_2, \tag{87}$$

and

$$C_{12}(|0\rangle_1|1\rangle_2 \pm |1\rangle_1|0\rangle_2) = (|0\rangle_1 \pm |1\rangle_1)|1\rangle_2. \tag{88}$$

These operations are essential for quantum teleportation.

One may recall that a classical NOT gate is called *universal* in the sense that any other logic gate may be created by combining several NOT gates. Similarly, a universal quantum gate should generate all unitary transformations of *n* qubits. It can be shown that such a gate is realized by combining a pair of gates, namely, one that produces a general rotation on a single bit, $U_{Universal}(\theta,\phi)$, where,

$$U_{Universal}(\theta,\phi) = \begin{bmatrix} \cos(\theta/2) & -ie^{-i\phi}\sin(\theta/2) \\ -ie^{i\phi}\sin(\theta/2) & \cos(\theta/2) \end{bmatrix}, \tag{89}$$

and a CNOT gate [100].

2.4.2 Quantum Teleportation

According to Bennett *et al.* [106], quantum teleportation is "a process that disembodies the exact quantum state of a particle into classical data and EPR correlations, and then uses these ingredients to reincarnate the state in

another particle which has never been anywhere near the first particle." The process does not involve sending any qubits, rather, the sender and the receiver must have access to two other resources, namely, the ability to send classical information, and an entangled EPR pairs of particles previously shared between them.

As per the sketch of Figure 2-13, teleportation proceeds as follows.

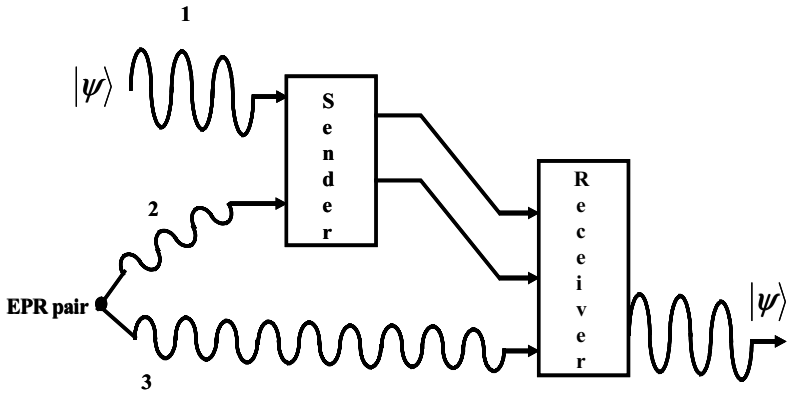

Figure 2-13. Quantum teleportation of state $|\psi\rangle$. (*After* [108].)

There are three particles involved, namely, particle 1, whose unknown state $|\psi\rangle = a|0\rangle_1 + b|1\rangle_1$ (a and b are the unknowns) is to be teleported by a *sender* to a *receiver*, and particles 2 and 3, which are prepared by an EPR source into an entangled EPR state, for instance,

$$|\Phi_{23}^{+}\rangle = \frac{\left(|0\rangle_2|0\rangle_3 + |1\rangle_2|1\rangle_3\right)}{\sqrt{2}}. \tag{90}$$

Of these two entangled particles, one, namely, particle 3, is sent by the EPR source to the receiver and the other, particle 2, is supplied to the sender. Notice that *locally* both the sender and the receiver possess total knowledge of the states of particles 2 and 3, respectively. However, *globally*, the three states are described by tensor product state,

$$|\psi_{123}\rangle = \frac{\left(a|0\rangle_1 + b|1\rangle_1\right)\left(|0\rangle_2|0\rangle_3 + |1\rangle_2|1\rangle_3\right)}{\sqrt{2}}, \tag{91}$$

consisting of the entangled pair, particles 2 and 3, and the unknown state. Now, the specific actions that effect the teleportation are as follows. The

sender performs a joint (XOR) measurement between particles 1 and 2. As we saw previously, the outcome of measuring a pair of single product states of two qubits, such as that of particles 1 and 2, has four possible outcomes

$$\left|\Psi^{\pm}\right\rangle_{12} = \frac{\left(\left|0\right\rangle_1\left|0\right\rangle_2 \pm \left|1\right\rangle_1\left|1\right\rangle_2\right)}{\sqrt{2}}, \tag{92}$$

and

$$\left|\Phi^{\pm}\right\rangle_{12} = \frac{\left(\left|0\right\rangle_1\left|1\right\rangle_2 \pm \left|1\right\rangle_1\left|0\right\rangle_2\right)}{\sqrt{2}}. \tag{93}$$

Taking this into account, the direct product state $\left|\psi_{123}\right\rangle$ may be expanded in terms of these four outcomes and rewritten as,

$$\begin{aligned}\left|\psi_{123}\right\rangle &= \frac{\left(a\left|000\right\rangle_{123} + a\left|011\right\rangle_{123} + b\left|100\right\rangle_{123} + b\left|111\right\rangle_{123}\right)}{\sqrt{2}} \\ &= \frac{1}{2}\left|\Phi^{+}\right\rangle_{12}\left(a\left|0\right\rangle_3 + b\left|1\right\rangle_3\right) + \frac{1}{2}\left|\Phi^{-}\right\rangle_{12} \\ &\quad \cdot\left(-a\left|0\right\rangle_3 + b\left|1\right\rangle_3\right) + \frac{1}{2}\left|\Psi^{+}\right\rangle_{12}\left(b\left|0\right\rangle_3 + a\left|1\right\rangle_3\right) \\ &\quad + \frac{1}{2}\left|\Psi^{-}\right\rangle_{12}\left(-b\left|0\right\rangle_3 + a\left|1\right\rangle_3\right)\end{aligned}. \tag{94}$$

The result of performing the XOR between particles 1 and 2 will be the *collapse* or projection of the *global* tensor product state $\left|\psi_{123}\right\rangle$ along one of the four vector states $\left|\Psi^{\pm}\right\rangle_{12}$ and $\left|\Phi^{\pm}\right\rangle_{12}$ with equal probability, namely, ¼. Notice that this will leave a new global state consisting of the tensor product of one of the vectors $\left|\Psi^{\pm}\right\rangle_{12}$ and $\left|\Phi^{\pm}\right\rangle_{12}$, *at the sender*, and a modified qubit 3, *at the receiver.* One possible result might be,

$$\left|\Psi^{+}\right\rangle_{12}\left(b\left|0\right\rangle_3 + a\left|1\right\rangle_3\right). \tag{95}$$

If these were the case then, to complete the teleportation process the sender has to communicate to the receiver, using classical message, that the global

wave function collapsed along $\left|\Psi^{+}\right\rangle_{12}$, and that for its qubit to embody the unknown state and, hence, complete the teleportation, it has to effect the unitary transformations: $\left|0\right\rangle_3 \rightarrow \left|1\right\rangle_3$ and $\left|1\right\rangle_3 \rightarrow \left|0\right\rangle_3$ on its qubit 3.

2.4.3 Decoherence

A quantum system is said to decohere when, in the course of its time evolution, it loses energy to the environment. Under these circumstances its transition matrix, *U*, no longer conserves the norm of the states it acts upon. Since the states change in a random manner, the property of superposition of states is no longer maintained. From thermodynamics we know that systems that experience energy loss are irreversible, therefore, decoherence precludes the realization of quantum gates, e.g., the Toffoli gate, which must be reversible. The ability of a quantum system to maintain its coherence and, thus, be capable of manifesting superposition and entanglement, is captured by the *decoherence time*. Obviously, the system is useful for quantum information processing only during this period of time. A system made up of many qubits will exhibit a compounded amount of errors as it approaches its decoherence time., i.e., as it becomes irreversible. The decoherence of a qubit, in particular, is quantitatively captured by the *quality factor of quantum coherence* [112],

$$Q_{\varphi} = \pi \nu_{01} T_{\varphi}, \tag{96}$$

where ν_{01} is its transition frequency and T_{φ} is the coherence time of a superposition of states. While error-correcting codes techniques have been proposed to combat errors stemming from decoherence, the need for an intrinsically coherent system to begin with, remains. Therefore, the conception of approaches exhibiting long decoherence times, with respect to the intended computational function to be implemented, is crucial, if quantum information processing is to become practical. Vion *et al.* [112] point out that, given a quantum computation with elementary operations taking time t_{op}, active compensation of deciherence requires Q_{φ}'s greater than $10^4 \nu_{01} t_{op}$. A number of approaches to the physical implementation of qubits, and their respective decoherencetimes, are discussed in Chapter 4.

2.5 Summary

This chapter has dealt with physical phenomena exploiting wave-particle duality. We began by addressing conditions that manifest charge discreteness, and its consequences on the performance of transmission lines, namely, persistent currents and current exhibiting Coulomb blockade (pulsating) behavior. Then, after introducing the concepts of single-electron tunneling, the effect of charge discreteness in electrostatic actuation was presented. In this context, we saw that charging dominated by Coulomb blockade may lead to quantized electrostatic actuation. Following this, we addressed the manifestation of quantum electrodynamical forces, in particular, van der Waals and Casimir forces and their substantial influence in moving nano- and micro-meter-scale devices. The chapter concluded with an exposition of the salient points of quantum information theory, computing and communications. In particular, we focused on the concepts of quantum bits, quantum entanglement, the Einstein-Podolsky-Rosen (EPR) state, quantum gates, and quantum teleportation. Lastly, the crucial issue of decoherence was discussed.

http://www.springer.com/978-1-4020-3238-7

Principles and Applications of NanoMEMS Physics

Santos, H.

2005, XVI, 254 p., Hardcover
ISBN: 978-1-4020-3238-7